SPE-198998-MS

The Effect of Osmotic Pressure on Improve Oil Recovery from Fractured Shale Formations

Perapon Fakcharoenphol, Colorado School of Mines, Basak Kurtoglu, Marathon Oil Company, Hossein Kazemi, Sarinya Charoenwongsa, and Yu-Shu Wu, Colorado School of Mines

This paper was prepared for presentation at the SPE Unconventional Resources Conference – USA held in The Woodlands, Texas, USA, 1-3 April 2014.

Abstract

Shale swelling during drilling is attributed to osmotic pressure, where low-salinity water enters the shale pores to cause swelling. Low-salinity water injected into high-salinity Bakken formation could similarly enter the matrix pores to displace oil by counter-current flow observed in core experiments. As a result, we believe, low-salinity water can potentially enhance oil recovery from oil-wet Bakken formation.

In this paper, we report experimental and numerical modeling studies we conducted to evaluate the potential of low-salinity waterflooding in Bakken. For laboratory experiments, we used horizontal core plugs drilled parallel to the bedding plane.

The mathematical included osmotic pressure, gravity and capillary effects. In the mathematical model, the osmotic pressure mass transfer equations were calibrated by matching time-dependent salinities in a published laboratory osmotic pressure experiment. We also modeled oil recovery for a Bakken core using our osmotic pressure mass transport model. The results indicate that osmotic pressure promotes counter-current flow of oil from both the water-wet and oil-wet segments of the core.

Introduction

Osmosis is the transport of water molecules flow from low-salinity side of a semi-permeable membrane to the high-salinity side to equalize the concentration of the dissolved salts. This causes an increase of pressure on the higher-salinity side, called osmotic pressure (π), **Fig. 1**. In subsurface environment, high-clay shale sediments can behave as a semi-permeable membrane, thus causing osmotic water transport (Kemper; 1961, Milne et al.; 1964, Young and Low; 1965, Chenevert; 1970, Olsen; 1972, Greenberg et al.; 1973, Marine and Fritz; 1981, Fritz; 1986, Van Oort et al.; 1994, and Keijzer; 2001).

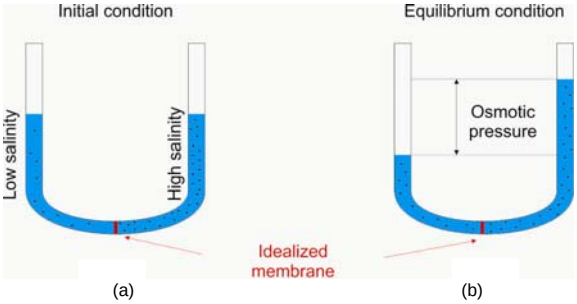

Fig. 1 – Illustration of osmotic pressure: (a) initial condition and (b) equilibrium condition

Marine and Fritz (1981), Neuzil (2000), and Neuzil and Provost (2009) reported that high-pressure anomalies in geological formations could be osmotic pressure. Furthermore, high salinity brine in some formations could be explained by reverse osmosis because during burial, porous rock is continuously compressed by the increasing overburden weight (de Sitter; 1947 and Bredehoeft et al.; 1963). Consequently, water molecules expel from the formation leaving salt behind. Because high-salinity brine, up to 280,000 ppm is found in shale formations, it may indicate semi-permeable membrane property of the shale (Kurtoglu; 2013).

Clay as Semi-Permeable Membrane

The electric double layer (EDL), diffused layer (DL), could explain the semi-permeable membrane property of shale and neutral zone (NZ) formed between pore body and the negatively charged clay surfaces, **Fig. 2**. The DL imposes an electrical repulsive force on anions; and to maintain electro-neutrality outside the DL, cations will remain with their co-ions. As a result, only charge-neutral water molecules can flow through the pore center (Mitchell; 2005 and Keijzer; 2000).

Additionally, there are uncharged membranes, which behave as sieves (Keijzer and Loch, 2001). That is, smaller particles are not restricted when flowing through such a membrane but bigger ones are. Olsen (1972) and Whitworth (1993) state that kaolinite and chalks may behave as efficient semi-permeable membrane based on pore size distribution.

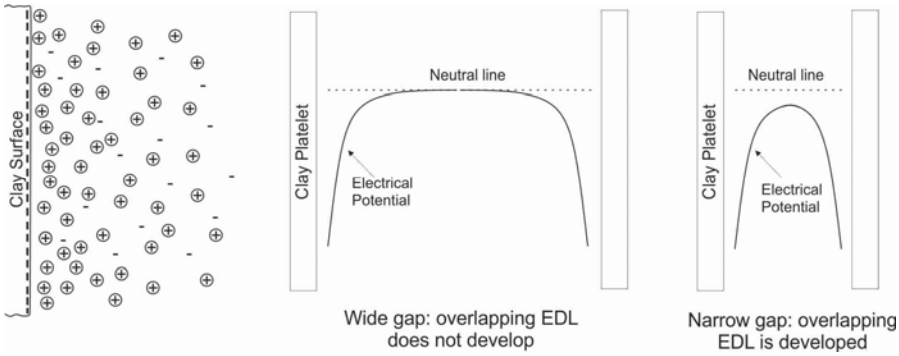

(a) (b) (c)

(a) electrical charge distribution near clay surface, (b) electric potential profile of a wide gap between two clay platelets with no overlapping diffuse layer (DL), and a neutral zone. The latter portrays pores in conventional reservoirs, which allows charged particles to pass through. (c) electrical potential profile in a narrow space between two clay platelets, as in unconventional pore space, having overlapping DL, which resists passage of charged particles while allowing the neutral particle migration.

Fig. 2 – Diagram showing electric double layer (EDL) next to the clay surface, the diffuse layer (DL), and the neutral zone (NZ) (adopted from Mitchell; 2005 and Keijzer; 2000)

Membrane Efficiency in Shale

Shale is very heterogeneous comprised of fine-grained sediments, with a wide range of compositions including kerogen, clay, quartz, feldspar, pyrite, heavy mineral. Prolific shale formations may contain high-clay content up to 80% (Bohacs et al., 2013). Shale also exhibits a wide range of pore-size distribution, **Fig. 3-a**. Kuila and Prasad (2011) reported three class of pore size in shale formations. The macro pores (diameter > 1000 nm) are predominately fractures, microfractures, and space between aggregates of clay. Meso-pores (diameter 10 – 100 nm, **Fig. 3-b**) comprise mainly the space between clay particles and within kerogen. Micro-pore (pore diameter < 10 nm) is intercrystalline pores between clay platelets.

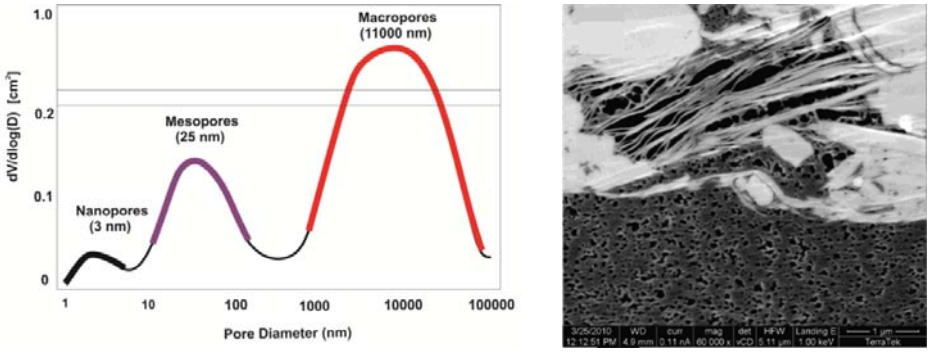

(a) (b)

Fig. 3 – Pores in shale formations: (a) three pore-size distribution for a shale samples (Kuila and Prasad, 2011), (b) ion-milled SEM image of meso-pores in kerogen and in clay for a Barnett shale sample (Milner et al., 2010).

Because of the wide pore-size range, shale can act as a non-ideal semi-permeable membrane, which only restricts the passage of some of the solutes in the solvent. As a result, pressure increase across the membrane does not reach the theoretical high osmotic pressure. For instance, Neuzil and Provost's (2009) review of public experimental data revealed a consistent low-membrane efficiency (less than 5%), which was defined as the measured pressure increase across the membrane divided by the theoretical osmotic pressure. Confining stress increases membrane efficiency. For instance, Rahman et al. (2005) reported an

increase in membrane efficiency from 14% at confining pressure of 1,000 psi to 39% at confining pressure of 4,000 psi.

Fig. 4 illustrates the clay-pore leakage mechanism as the cause of osmotic pressure. Initially, the pore space between clay particles and within the clay structure is full of high-salinity formation brine. Once low-salinity water contacts the clay particles, osmotic force induces flow of water molecules into the clay structure through the small meso-pore between clay particles to cause EDL overlap and reduction of salinity in the pore. Furthermore, pressure inside the pore increases (osmotic pressure) and expels some of the water and salt through the larger pore. This is why the laboratory-measured osmotic pressure is not as high as the theoretical osmotic pressure of a perfect membrane. Nonetheless, at the nano-scale level, the pressure that cause flow across the overlapping EDLs may be as high as the theoretical osmotic pressure.

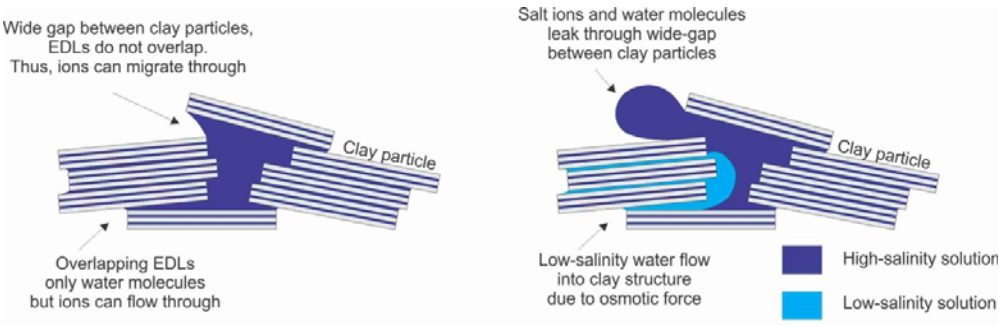

Fig. 4 – Schematic showing membrane leakage mechanism for clays: (a) Pore space initially filled with high-salinity water. (b) Low-salinity water flows into the clay structure due to osmotic force, and high-salinity water leaves through a pore gap larger than clay sheet spacing.

Osmotic Pressure-Induced Flow in Multiphase System in Shale Formations

In hydrocarbon-producing shale, the bulk of movable fluids in the shale matrix include oil and gas while high-salinity brine is either trapped or bound to clays. Water flowback data indicates that the salinity of formation brine can be as high as 280,000 ppm or 28% by weight in some shale formations (Kurtoglu, 2013). Because typical fracturing fluids comprise of low-salinity (e.g., 10,000 ppm) water, significant salinity contrast exists between injected and formation water. This salinity contrast can cause a substantial osmotic pressure gradient to drive fracturing fluid into the shale matrix via surrounding fractures.

Fig. 5 is a schematic of the osmotic-induced flow in shale containing oil and water. Initially, oil occupies most of the pore space while formation water is bound to the clay platelets (**Fig. 5-a**). Once low-salinity water contacts the clays, low-salinity water molecules enter the nano-pore space within the clay structure. As a result, clay swells and pore pressure increases to expel oil through larger meso-pores (**Fig. 5-b**).

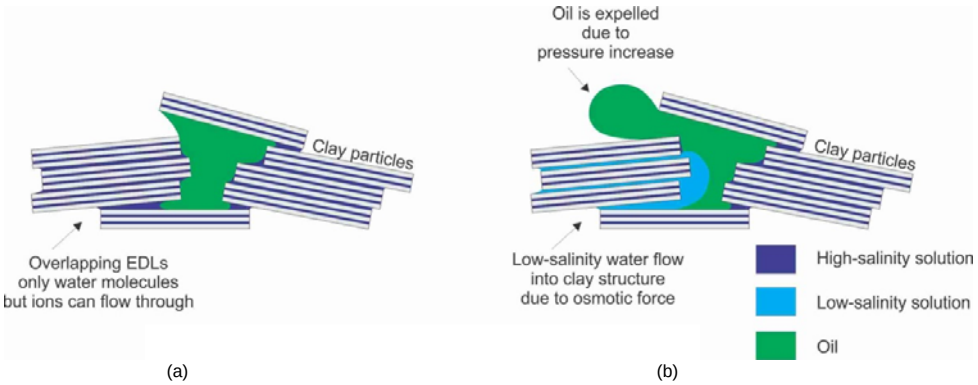

Fig. 5 – Schematic showing oil-water flow in shale: (a) Pore space at the initial condition where the bulk of the movable fluid is oil while high-salinity brine is bound to clay sheets. (b) Clay in contact with low-salinity water, which has broken through some clay structure to push oil out of meso-pores.

Interestingly, some shale formations are oil-wet because of Ca2+/Na+ bridging of oil molecules to the negatively charged clay surface. The invaded low-salinity water dilutes salt concentration in the formation brine and causes detachment of Ca2+/Na+ from the clay surface (Kurtoglu, 2013). As a result, the surface may become water-wet, causing an increase in relative permeability of oil and a reduction of irreducible oil saturation; thus, leading to improved oil production.

Mineralogy and pore structure in Bakken

When we talk about shale pores as membranes, we need to examine shale pore structure and mineralogy to see whether they fit the membrane theoretical requirements. Thus, we present the mineralogy and pore structure of Bakken formation in **Fig. 6**.

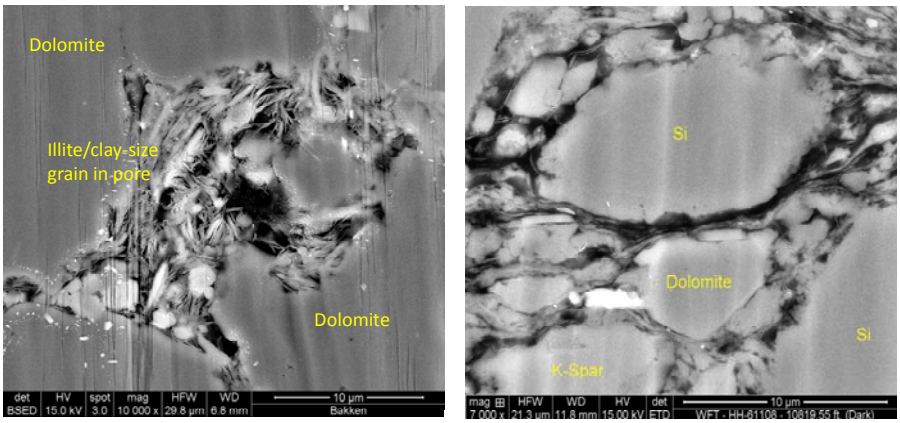

(a) (b)

Fig. 6 – Mineralogy and pore structure of Bakken formation: (a) Ion-milled SEM of oil producing Middle Bakken. (b) Ion-milled SEM of source rock in Lower Bakken (Kurtoglu, 2013).

Oil Recovery Experiments

We performed low and high-salinity imbibition experiments using a laminated Middle Bakken formation core. **Fig. 7-a**, Bakken 282,000 ppm high-salinity (**Table 1**) experiment, shows only a few oil droplets on the core surface at day five. We removed the core from the imbibition cell and put it into another cell filled with 20,000-ppm KCl brine. **Fig. 7-b** shows the low-salinity imbibition results after one day, which indicates that the low-salinity brine has greater spontaneous imbibition with more oil droplets forming on the core surface. Much of the oil appeared along the core laminations.

With the high-salinity brine inside and outside of the core, EDL overlap does not develop to expel oil from pores. When clay particles are exposed to the low-salinity brine, osmotic force causes flow of the water molecules into the clay pore space, causing an EDL overlap to expel oil from the clay-rich laminations.

(a) (b)

Fig. 7 – Spontaneous imbibition experiments: (a) high-salinity formation water at the end of Day 5, (b) low–salinity brine at the end of Day 6 (Kurtoglu, 2013).

.

Mathematical model

Mathematical description of osmosis-induced flow in single-phase porous media has been well documented. (Abdel-Aziz and Taylor, 1964; Olsen, 1972; Neuzil, 1986; van Oort et al., 1995; Keijzer, 2000; and Mitchell and Soga, 2005). Specifically, Olsen (1972) compared chemical and electrical osmosis flow to the pressure-induced flow in subsurface environment, and Greenberg et al. (1973) modeled seawater intrusion in California using chemical osmosis concepts.

In this paper, we present a multi-phase, chemical osmosis, flow model for hydrocarbon-bearing shale formations. We modeled solute transport by a single component. We created osmotic pressure as a function of salt concentration in the same manner as capillary pressure and relative permeability saturation functionality.

Osmotic Pressure Calculation

Marine and Fritz (1981) described osmotic pressure (π) by Eq. 1:

$$\pi = \frac{RT}{V}\ln\left(\frac{a_I}{a_{II}}\right) \quad (1)$$

Where a_I , a_{II} are water activities of low-salinity brine I and high-salinity brine II; Water activity for fresh water is 1.0; R gas constant equal to 0.082 (liter.atm)/(g-mol.°K); T temperature in °K, and V molar volume in liter/g-mol.

Water activity can be calculated from the Helgeson-Kirkham-Flowers (HKF) equation of state (Helgeson et al., 1981). In high-solute concentration and high-temperature systems, the calculation requires an iterative computational procedure (Helgeson et al.; 1981 and Xu et al.; 2012). We used TOUGHREACT simulator to generate brine activity values using a single-grid model. Because water activity of fresh water is one, Eq. 1 becomes:

$$\pi = -\frac{RT}{V}\ln\left(a_{II}\right) \quad (2)$$

Salt Concentration-Osmotic Pressure Curves

Assuming a perfect semi-permeable membrane, we constructed a plot of the salt concentration versus osmotic pressure to investigate the effect of temperature and water composition on osmotic pressure as an input to the flow simulator.

TABLE 1 – BAKKEN FLOW BACK WATER*

Ion	Concentration (ppm)	Molality (mol/liter)
Ca^{2+}	20,507	0.51
Mg^{2+}	1,491	0.06
Na^{+}	85,994	3.74
Cl^{-}	174,733	4.92
Total Salinity	282,725	

* Obtained from Kurtoglu (2013)

Fig. 8-a presents calculated osmotic pressure of the Bakken flow back brine (**Table 1)** at temperature of 212 °F and 284 °F. For comparison, **Fig. 8-b** is the computed osmotic pressure for sodium chloride (NaCl) and calcium chloride ($CaCl_2$) solutions**.** The results indicate that water composition significantly affects osmotic pressure. Osmotic pressure of sodium chloride solution is much higher than that of calcium chloride solution.

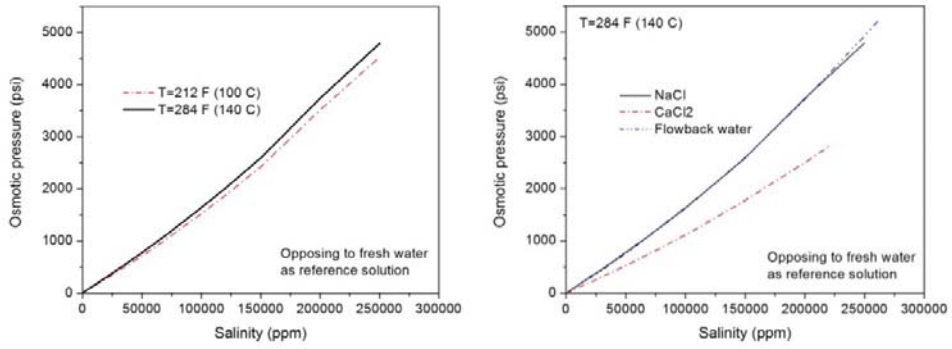

Fig. 8 – Bakken osmotic pressure: (a) Reservoir temperature 212 °F and 284 °F. (b) NaCl vs. CaCl2 solution. (Water composition was obtained from Kurtoglu; 2013).

Single-Phase Flow in Porous Media

Olsen (1972) described single-phase flow of water in shale by the Darcy flow enhanced by osmotic pressure, Eq. 3:

$$\vec{v} = -\frac{k}{\mu}\left[\nabla p - \gamma\nabla D - E_{op}\nabla\pi\left(C\right)\right] \quad (3)$$

where k is permeability, μ fluid viscosity, p pressure, γ fluid gradient, D depth which is positive downward, π osmotic pressure which is calculated from salt concentration C, and E_{op} osmotic efficiency.

Solute transport through small meso-pores is controlled by the semi-permeable membrane property of shale as discussed

in the previous section. Thus, solute molecules move by (1) advection pressure gradient through large pores , and (2) diffusion $\left(\vec{F}^{diff}\right)$ concentration gradient.

Advection:

$$\vec{F}^{adv} = C^p \rho^p \vec{v}^p \tag{4}$$

where C^p , ρ^p and $\vec{v}^p$ are solute concentration and density, while $\vec{v}^p$ is the Darcy flux vector, Eq. 5:

$$\vec{v}^p = -\frac{k}{\mu}\left(\nabla p - \gamma \nabla D\right) \tag{5}$$

Eq. 6 describes the net diffusion flux:

$$\vec{F}^{diff} = -\left(1 - E_{op}\right) D \nabla C \tag{6}$$

where D is effective diffusion coefficient.

Eq. 7 and Eq. 8 are the mass transport equations for water (solvent) and solute (salt) in shale, which we used in our model:

Water:

$$-\nabla \cdot \rho \vec{v} + \rho \hat{q} = \frac{\partial \rho \phi}{\partial t} \tag{7}$$

where, $\hat{q}$ is sing/source term per unit volume, porosity, and t time.

Solute:

$$-\nabla \cdot \vec{F}^{adv} - \nabla \cdot \vec{F}^{diff} + C \rho \hat{q} = \frac{\partial C \rho \phi}{\partial t} \tag{8}$$

Simulating an Osmotic Pressure Mass Transport Experiment

To test the validity of our osmotic pressure mathematical model, we matched osmotic pressures measured on a shale sample experiment, conducted by Takeda et al. (2012). The sample, siliceous shale cut from a core taken at depth of 982 m, was 5 cm in diameter and 1 cm in thickness. Separate sodium chloride reservoirs were connected to the top and bottom of the sample. The top reservoir contained 0.1 mol/liter salt solution while the bottom reservoir contained 0.55 mol/liter solution. In the experiment, Takeda et al. measured pressure and salt concentration at discrete time intervals, which we used to match the numerical model calculations. The numerical model was a vertical 1-D finite-difference simulator consisting of seven grid cells. The first grid cell represented the sodium chloride reservoirs at the bottom while the seventh cell was the sodium chloride reservoir at the top. The remaining five grid cells represented the shale sample. **Table 2** contains the details of the model input parameters, while **Fig. 9-a** and **9-b** show the comparison between experiment and modeling results.

The simulation results indicate that the pressure in the bottom cell sharply increases due to flow of low-salinity brine, by osmotic pressure gradient, from the top cell. The counter-current flow and diffusion of salt molecules decrease salt concentration in the bottom reservoir. To achieve a match, we used an osmotic pressure membrane efficiency of 0.05 (five percent).

TABLE 2 – INPUT PARAMETERS FOR THE SINGLE-PHASE FLOW MODEL

	Bottom reservoir	Rock	Top reservoirs
Rock properties			
Volume, ft^3	7.417×10^{-3}	6.923×10^{-3}	3.532×10^{-3}
Initial pressure, psi	42.5	42.5	42.5
Initial concentration, mol/liter	0.55	0.1	0.1
Porosity, fraction		0.28	
Permeability, mD		1.54×10^{-4} *	
Interface area, ft^2	0.021	0.021	0.021
Length, ft		0.032	
Effective diffusion coefficient, ft^2/day		2.487×10^{-5} **	
Discretization	1×1×1	5×1×1	1×1×1
Matching parameters			
Osmotic efficiency, fraction		0.05	

* Takeda et al. (2012)
** Rahman et al. (2005)

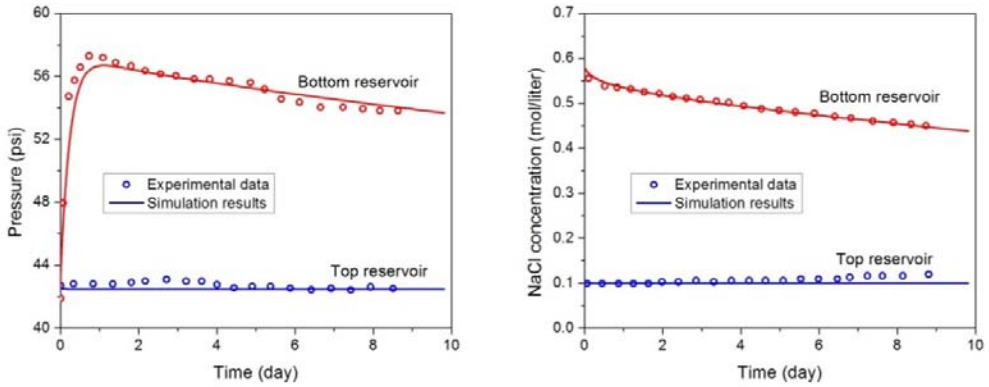

(a) (b)

Fig. 9 – Comparison between numerical simulation results and experimental data of Takeda et al. (2012): (a) pressure and (b) salt concentration.

Multi-Phase Flow in Fractured Shale Formations

Micropore ($d \le 2\ nm$), mesopore ($2\ nm \le d \le 50\ nm$), and macropore ($d \ge 50\ nm$) are common designations of shale pore-size distribution. The macropores represent predominately fractures and micro-fractures, while mesopores and micropores represent two main pore classes in the shale matrix (Kuila and Prasad, 2011). Consequently, we can formulate fluid-flow in shale using a double-porosity model, where fractures form the continuum of interconnected fracture network while the shale matrix become the discrete medium embedded in the fracture continuum.

The commonly used transfer function τ, used to describe mass transport between fracture and matrix in dual-porosity modeling (Kazemi and Gilman, 1993) can be extended to chemical osmosis mass transport. The following equations describe the modifications for the water-oil flow:

Water:

$$\tau_{w,f/m} = \tau^{p}_{w,f/m} + \tau^{\pi}_{w,f/m} \tag{9}$$

where $\tau^{p}_{w,f/m}$ and $\tau^{\pi}_{w,f/m}$ are transfer functions of water induced by pressure and osmotic pressure, respectively. The following equations describe $\tau^{\pi}_{w,f/m}$ and $\tau^{p}_{w,f/m}$:

$$\tau^{\pi}_{w,f/m} = -\sigma_{f/m} k_m \lambda_{w,f/m} E_{op} \left[\pi_f \left(C_f \right) - \pi_m \left(C_m \right) \right] \tag{10}$$

where $\sigma_{f/m}$ is shape factor for flow between fracture and matrix , k_m shale matrix permeability, and $\lambda_{w,f/m}$ water mobility.

And,

$$\tau^{p}_{w,f/m} = \sigma_{f/m} k_m \lambda_{wf/m} \left[\left(p_{of} - p_{om} \right) - \left(p_{cowf} - p_{cowm} \right) + \frac{\sigma_{z,f/m}}{\sigma_{f/m}} \gamma_w \left(h_{wf} - h_{wm} \right) \right] \tag{11}$$

where p_{of} and p_{om} are the oil pressure in fracture and matrix, p_{cowf} and p_{cowm} the capillary pressure of water-oil system in fracture and matrix, $\sigma_{z,f/m}$ shape factor for flow in vertical direction, h_{wf} and h_{wm} water column height in fracture and matrix (Kazemi and Gilman, 1993).

Oil:

$$\tau_{o,f/m} = \sigma_{f/m} k_m \lambda_{of/m} \left[\left(p_{of} - p_{om} \right) - \frac{\sigma_{z,f/m}}{\sigma_{f/m}} \gamma_o \left(h_{wf} - h_{wm} \right) \right] \tag{12}$$

Governing equations for water-oil system in fractured shale formations are given:

Mass balance in fracture:

Water:

$$-\nabla\cdot\left(\rho_w\vec{v}_w\right)_f+\rho_w\hat{q}_w-\rho_w\tau_{w,f/m}=\frac{\partial\left(\rho_wS_w\phi\right)_f}{\partial t} \tag{13}$$

Oil:

$$-\nabla\cdot\left(\rho_o\vec{v}_o\right)_f+\rho_o\hat{q}_o-\rho_o\tau_{o,f/m}=\frac{\partial\left(\rho_oS_o\phi\right)_f}{\partial t} \tag{14}$$

Salt:

$$-\nabla\cdot\left(\vec{F}^{adv}\right)_f-\nabla\cdot\left(\vec{F}^{diff}\right)_f+C\rho_w\hat{q}_w-F^{adv}_{f/m}-F^{diff}_{f/m}=\frac{\partial\left(C\rho_wS_w\phi\right)_f}{\partial t} \tag{15}$$

where $F^{adv}_{f/m}$ and $F^{diff}_{f/m}$, defined below, are salt transport between fracture and matrix by advection and diffusion, respectively.

$$F^{adv}_{f/m}=C_{f/m}\rho_w\tau^{p}_{f/m}+C_{f/m}\rho_w\tau^{\pi}_{f/m} \tag{16}$$

and

$$F^{diff}_{f/m}=\left(1-E_{op}\right)\sigma D_{f/m}\left(C_f-C_m\right) \tag{17}$$

where $C_{f/m}$ salt concentration in fracture or matrix, and $D_{f/m}$ effective diffusion coefficient between fracture and matrix.

Mass balance in matrix:

Water:

$$\rho_w\tau_{w,f/m}=\frac{\partial\left(\rho_wS_w\phi\right)_m}{\partial t} \tag{20}$$

Oil:

$$\rho_o\tau_{o,f/m}=\frac{\partial\left(\rho_oS_o\phi\right)_m}{\partial t} \tag{21}$$

Salt:

$$F^{adv}_{f/m}+F^{diff}_{f/m}=\frac{\partial\left(C\rho_wS_w\phi\right)_m}{\partial t} \tag{22}$$

The Effect of Chemical Osmosis on Oil and Gas Production

We used a 1-D dual-porosity model to simulate the effect of chemical osmosis on oil and gas production in shale formations. Matrix was a sugar cube with a linear dimension of 10 feet. The simulation starting point is after a single-staged hydraulic-fracture stimulation operation. In the simulation, the fracturing fluid has a salinity of 10,000 ppm. Thus, the fracture network also contains low-salinity fracturing fluid with 10,000-ppm salt concentration at all times. The 1-D simulation results were up-scaled to a one-square-mile multi-stage well pattern. The simulation assumptions are:

- Fracture pressure, water saturation, and salt concentration are constant while matrix pressure, water saturation and salt concentration are changed with time.
- Oil production from the matrix immediately reaches the producers once leaving the matrix.
- Matrix wettability alteration due to the change in salt concentration is ignored.
- No fracture and matrix permeability change throughout the simulation.

We used the relative permeability data (**Fig. 10-a**) that a service company had measured on a Bakken core. We also constructed the capillary pressure function (**Fig. 10-b**) based on numerous published laboratory measured drainage data. **Table 3** presents the remaining input parameters for the model. We modeled six simulation scenarios (**Table 4**) with different shale-membrane efficiency and wettability to investigate their effect on well production.

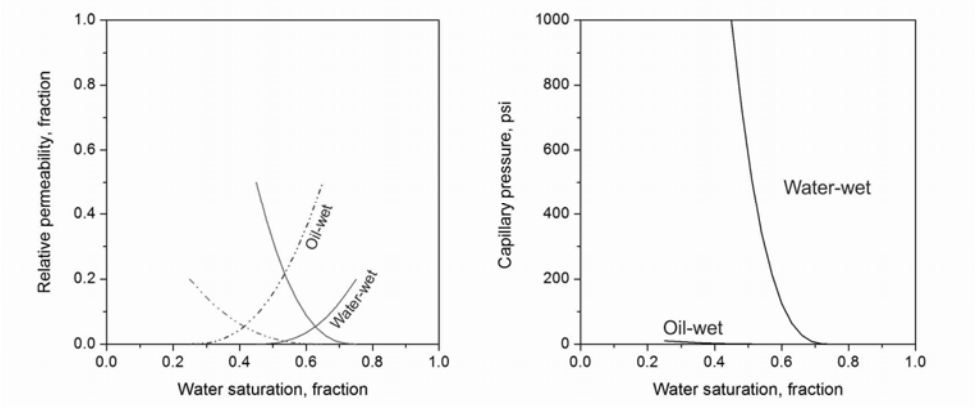

(a) (b)

Fig. 10 – Rock properties: (a) relative permeability and (b) capillary pressure.

TABLE 3 – INPUT PARAMETERS FOR THE MULTI-PHASE FLOW MODEL

	Fracture	Shale matrix
Initial salt concentration, ppm	10,000	250,000
Initial water saturation, fraction	1.00	0.28 (oil-wet) 0.48 (water-wet)
Irreducible water saturation, fraction		0.25 (oil-wet) 0.45 (water-wet)
Porosity, fraction		0.08
Permeability, mD		1.0×10^{-3}
Shape factor, ft^{-2}		0.12 (10 ft. matrix block)
Effective diffusion coefficient, ft^2/day		1.0×10^{-6}
Osmotic efficiency, fraction		0.05
Drainage area, ft^2	5,280×5,280	
Thickness, ft	35	

TABLE 4 – SIMULATION CASE SUMMARY

Cases	Rock wettability	Osmotic efficiency
1	Oil-wet	1%
2	Oil-wet	5%
3	Oil-wet	10%
4	Water-wet	1%
5	Water-wet	5%
6	Water-wet	10%

Simulation Results

The simulation results of the oil-wet rock with a membrane efficiency of five percent (Case 2) are shown in **Fig. 11**. Water and oil flow rates reported in **Fig 11-a**. Initially, the flow rate between fracture and matrix is minimal because relative permeability to water in the matrix is low; however, after considerable time water penetrates into the matrix pores to cause higher flow rates.

The osmotic force induces flow from fracture to matrix (negative value). As a result, matrix pore pressure increases, **Fig. 11-b**. This increase causes flow from matrix to fracture. In turn, the flow reduces matrix pressure, thus only 40-psi pressure increase is observed. As the relative permeability to oil is higher than that of water, oil starts to flow from the matrix to fracture (positive value) at about 20 years. After 40 years of production, oil recovery factor from shale matrix could reach about 35 percent, **Fig. 11-d**.

Low-salinity water flowing from fracture flow into the matrix pores dilutes the matrix salt concentration (**Fig. 11-c**) and reduces the concentration contrast between fracture and matrix. As a result, it reduces the osmotic force. Thus, the osmotic-

induced water flow rate decreases.

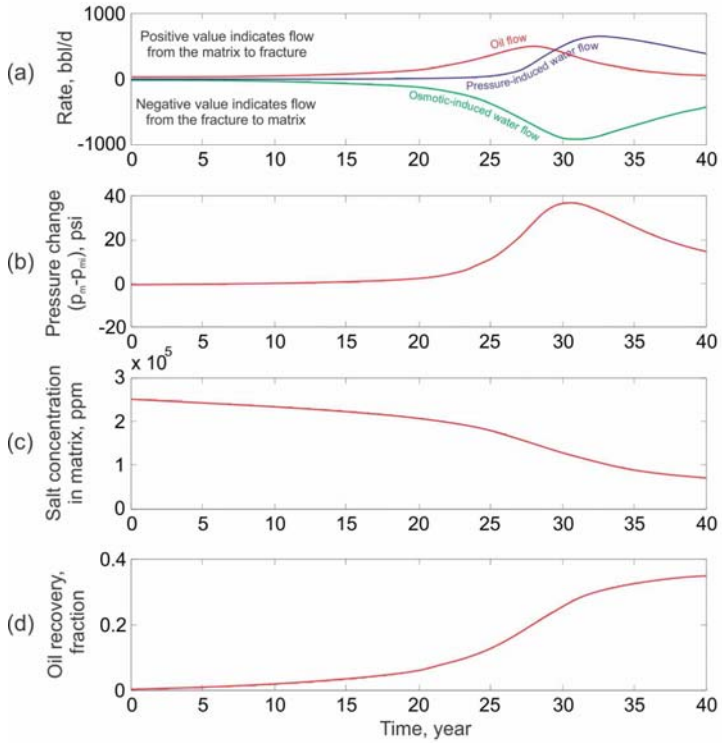

Fig 11 – Simulation results for Case 2: Oil-wet rock and osmotic efficiency of 5%: (a) pressure- and osmotic-induced water flow and oil flow rates, (b) Pressure change in shale matrix, (c) Salt concentration in shale matrix, and (d) oil recovery factor.

Wettability and Osmotic Efficiency Effects

Osmotic force is the only realistic force to overcome the negative capillary pressure of the oil-wet rock to cause counter-current flow of water from fracture into the matrix and oil into fractures. Thus, osmotic membrane efficiency could significantly affect economic oil production rates and recovery factor (**Fig. 12**) in oil-wet shale.

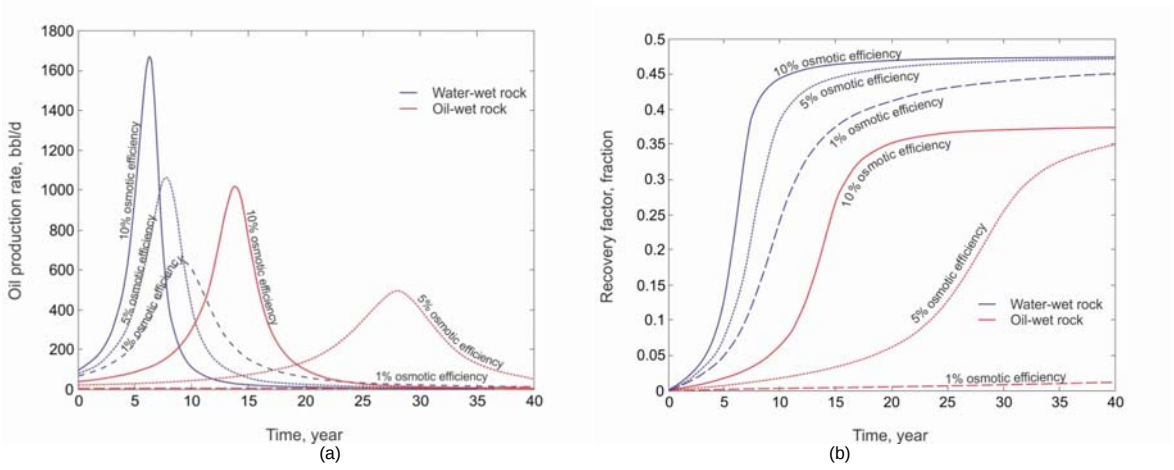

Fig 12 – Simulation results comparison: (a) oil production rate and (b) oil recovery factor

Conclusions

Hydrocarbon producing shale formations are oil wet because of abundance of kerogen in pore structure. Thus, brine should have a difficult time entering the shale pores. However, we have observed brine entering preserved core samples in the laboratory. We believe this is caused by osmotic pressure because of presence of clays and high-salinity brine in the shale pores. When shale is contacted with low-salinity brine, it enters shale pores by osmotic pressure created because of the salinity

contrast of the high-salinity brine in the pores and the low-salinity brine contacting the shale. We built a dual-porosity mathematical model to include this osmotic pressure in the model. In this study, we have arrived at the following conclusions:

1. Because of presence of clays and high-salinity brine in the shale pores, some hydrocarbon-bearing formations behave as osmotic membranes when contacted with low-salinity brine. Thus, low-salinity brine can potentially displace oil in oil-bearing shale formations. Similarly, in gas-bearing formations, when a gas well is shut in for several months after hydraulic fracturing, the gas rate will increase when the well is re-opened. We believe osmotic pressure can imbibe the hydraulic fracturing fluid, the "slickwater", to enhance gas production temporarily.

2. The mathematical model presented in this paper can simulate the osmotic pressure oil-recovery -- the underlying principle of the low-salinity water flooding. This oil recovery technique might yield economic amounts of incremental oil in suitable shale formations.

3. The osmotic pressure, caused by salinity contrast, can cause counter-current flow of water and oil both in oil-wet and water-wet porous formations. Thus, in conventional reservoirs, low-salinity oil recovery improvements of carbonate formations might be partly because of osmotic pressure induced by salinity contrast.

Acknowledgements

The authors acknowledge the support received from Marathon Center of Excellence for Reservoir Studies (MCERS) and Energy Modeling Group (EMG) at Colorado School of Mines and Marathon Oil Company. We also extend special gratitude to the following individuals at Marathon Technical Laboratory: Richard Rosen, Tobi Kosanke, and William Mickelson for their help in the experimental studies and interpretation.

Nomenclature

a	water activity [-]
C	salt concentration [-]
D	depth [L]
E_{op}	osmotic efficiency [-]
$\vec{F}$	mass flux rate [M/(L^{2}t)]
h	height of fluid column [L]
k	permeability [L^2]
p	pressure [M/(Lt^2)]
$\hat{q}$	fluid sink and source term per volume [1/t]
R	gas constant []
S	fluid saturation [-]
t	time [t]
T	temperature [T]
$\vec{v}$	Darcy velocity [L/t]
V	molar volume [L^3/m]

Greek Letters

ϕ	porosity [-]
γ	fluid gradient [M/(L^{2}t^2)]
μ	viscosity [M/(Lt)]
π	osmotic pressure [M/(Lt^2)]
ρ	density [M/L^3]
σ	shape factor [1/L^2]
τ	transfer function [1/t]

Operators

∇	Gradient operator
$\nabla\cdot$	Divergence operator
$\partial / \partial t$	time derivative [1/t]

Superscripts

adv	induced by advection
diff	induced by diffusion
p	induced by pressure
π	induced by osmotic pressure

Subscripts

cwo	capillary of a water and oil system
f	fracture
f / *m*	between fracture and matrix
m	matrix
o	oil phase
w	water phase
z	in vertical direction only

References

Abd-el-Aziz, M., and S. A. Taylor, 1964, Simultaneous flow of water and salt through unsaturated porous media, *Soil Sci. Soc. Amer. Proc*., 29(2), 141.

Alharthy, N., T, Teklu, H. Kazemi, and R. Graves, 2013, Multiphase Compositional Modeling in Small-Scale Pores of Unconventional Shale Reservoirs, In *UNGI Consortium Progress Meeting Proc*., Nov.

Bredehoeft, J. D., C. R. Blyth, W. A. White, and G. B. Maxey, 1963, Possible Mechanism for Concentration of Brines in Subsurface Formations, *AAPG Bulletin* 47(2): 257–269.

Bohacs, K., Q. Passey, M. Rudnicki, W. Esch and O. Lazar, 2013, The Spectrum of Fine-Grained Reservoirs from 'Shale Gas' to 'Shale Oil'/ Tight Liquids: Essential Attributes, Key Controls, Practical Characterization, IPTC-16676, In *6th International Petroleum Technology Conference Proc.,* Beijing, China.

Chenevert, M.E., 1970, Shale Alteration by Water Adsorption, *JPT*, 1309–1316.

Greenberg, J. A., J. K. Mitchell, and P. A. Witherspoon, 1973, Coupled Salt and Water Flows in a Groundwater Basin, *Journal of*

Geophysical Research, 78: 6341–6353.
De Sitter, L. V., 1947, Digenesis of oil-field brines, *Am. Assoc. Pet. Geol. Bull*., 31(11):2030-2040.
Helgeson, H. C., D.H. Kirkham, G. C. Flowers, 1981, Theoretical prediction of the thermodynamic behavior of aqueous electrolytes by high pressures and temperatures; IV, Calculation of activity coefficients, osmotic coefficients, and apparent molal and standard and relative partial molal properties to 600 degrees C and 5kb, *American Journal of Science*, 281:1249–1516.
Kazemi, H. and J. R. Gilman, 1993, Multiphase Flow in Fractured Petroleum Reservoirs. *Flow and Contaminant Transport in Fractured Rocks*, Eds. J. Bear, C-F Tang, and B. De Marsily, 267-323, Academic Press.
Kemper, W. D., 1961, Movement of water as effected by free energy and pressure gradient II, Experimental analysis of porous systems in which free energy and pressure gradients act in opposite directions, *Soil Sci. Soc. Am. Proc*., 25(4): 260-265.
Keijzer, T. J. S., 2000, Chemical Osmosis in Natural Clayey Materials, *PhD thesis*, Utrecht University, Netherlands.
Keijzer, T. J. S., and J. P. G. Loch, 2001, Chemical Osmosis in Compacted Dredging Sludge, *Soil Sci. Soc. Am. J*., 65(4): 1045-1055.
Kuila, U. and M. Prasad, 2011, Surface Area and Pore-size Distribution in Clays and Shales, SPE-146869, In *2011 SPE ATCE Proc.*, Denver, Colorado, USA: Society of Petroleum Engineers.
Kurtoglu, B., 2013, Integrated Reservoir Characterization and Modeling in Support of Enhanced Oil Recovery for Bakken, *PhD thesis*, Colorado School of Mines, USA.
Marine, I. W., and S. J. Fritz, 1981, Osmotic Model to Explain Anomalous Hydraulic Heads, *Water Resources Research*, 17(1): 73–82.
Milner, M., R. McLin, and J. Petriello, 2010, Imaging Texture and Porosity in Mudstones and Shales: Comparison of Secondary and Ion-Milled Backscatter SEM Methods, SPE-138975, In *2010 Canadian Unconventional Resources and International Petroleum Conference Proc.*. Calgary, Alberta, Canada: Society of Petroleum Engineers, 2010.
Mitchell, J. K. and K. Soga, Fundamentals of Soil Behavior, 3rd edition, Hoboken, N.J.: John Wiley & Sons, 2005.
Milne, I. H., J. G. McKelvey, and R. P. Trump, 1964, Semi-permeability of bentonite membranes to brines, Am. *Assoc. Pet. Geol. Bull.*, 48(1):103-105.
Neuzil, C. E., 1986, Groundwater Flow in Low-Permeability Environments, *Water Resources Research* 22(8): 1163–1195.
Neuzil, C. E, 2000, Osmotic Generation of 'anomalous' Fluid Pressures in Geological Environments, *Nature*, 403: 182–184.
Neuzil, C. E., and A. M. Provost, 2009, Recent Experimental Data May Point to a Greater Role for Osmotic Pressures in the Subsurface, *Water Resources Research*, 45(3).
Olsen, H. W, 1972, Liquid Movement Through Kaolinite Under Hydraulic, Electric, and Osmotic Gradients, *AAPG Bulletin*, 56(10): 2022–2028.
Staverman, A. J., 1952, Non-equilibrium thermodynamics of membrane processes: *Faraday Soc. Trans.,* 48(2):176-185.
Takeda, M., T. Hiratsuka, K. Ito, and S. Finsterle, 2012, Development and Application of Chemical Osmosis Simulator Based on TOUGH2, In *2012 TOUGH2 Symposium Proc.*, Lawrence Berkeley National Laboratory, Berkeley, California, 2012.
van Oort, E., A.H. Hale, and F.K. Mody, 1995, Manipulation of Coupled Osmotic Flows for Stabilisation of Shales Exposed to Water-Based Drilling Fluids, SPE 30499, In *1995 SPE ATCE Proc.*, Dallas, Texas, Society of Petroleum Engineers.
Whitworth, T. M., 1993, Hyper-filtration-induced Isotopic Fractionation: Mechanisms and Role in the Subsurface, *Ph.D. thesis*, Purdue University, USA
Xu, T., N. Spycher, E. Sonnenthal, G. Zhang, L. Zheng, and K. Pruess, 2004, TOUGH-REACT User's Guide: A Simulator Program for Non-isothermal Multiphase Reactive Transport in Variably Saturated Geological Media, *Report LBNL-55460*, Lawrence Berkeley National Laboratory, Berkeley, Calif.
Young, A. and P. F. Low, 1965, Osmosis in Argillaceous Rocks: GEOLOGICAL NOTES, *AAPG Bulletin*, 49:1004–1007.